

**An experimental investigation of disturbance
growth in boundary layer flows**

by

Thomas Kurian

May 2010
Technical Reports from
Royal Institute of Technology
KTH Mechanics
SE-100 44 Stockholm, Sweden

Akademisk avhandling som med tillstånd av Kungliga Tekniska Högskolan i Stockholm framlägges till offentlig granskning för avläggande av teknologie doktorsexamen fredagen den 11 juni 2010 kl 10.15 i sal F3 vid Kungliga Tekniska Högskolan, Lindstedsvägen 26, Stockholm.

©Thomas Kurian 2010

Universitetsservice US-AB, Stockholm 2010

Thomas Kurian 2010, **An experimental investigation of disturbance growth in boundary layer flows**

Linné FLOW Centre, KTH Mechanics
SE-100 44 Stockholm, Sweden

Abstract

This thesis deals with the early stages of transition to turbulence in two different baseflows, namely the Falkner-Skan-Cooke boundary layer (FSC) and the asymptotic suction boundary layer (ASBL).

Grid-generated turbulence is studied in order to characterise the isotropy levels, free-stream turbulence levels and characteristic length scales that will be present in the receptivity study. By varying the grids and their location it is possible to control the turbulence intensity level, Tu , and the integral length scale independently. Comparisons with other studies show that for increasing Re_M the isotropy levels and the rate of kinetic energy decay asymptotically approach the theoretical values.

The FSC describes a 3D boundary layer subjected to a pressure gradient. The FSC is stable to TS-waves, but becomes susceptible to both travelling and stationary crossflow disturbances. In the experiments the travelling modes were triggered using free-stream turbulence (FST) and the stationary modes were triggered using an array of cylindrical roughness elements. The receptivity phase to FST was linear as well as the initial growth. For high enough Tu inside the boundary layer, nonlinear behaviour was observed further downstream. The stationary mode could only be triggered using tall roughness elements, with low heights resulting in no noticeable disturbances. The receptivity is found to be nonlinear for the roughness heights tested and the growth of the disturbances is exponential. For low levels of FST, $Tu < 0.25\%$, the travelling mode as well as the stationary mode grew.

The ASBL is formed when uniform suction is applied to the surface of a porous plate with a flow over it. This baseflow is very stable to TS-waves, and was used to study the transient growth. For the ASBL, stationary disturbances were triggered using a spanwise array of cylindrical roughness elements. The velocity signals were decomposed using a spatial Fourier transform to study the growth of individual modes. The fundamental mode as well as some harmonics were seen to undergo transient growth, before finally decaying exponentially.

Comparisons were made to the experimental data using optimal perturbation theory. The global optimals did not describe the transient growth effects well. The calculations were redone for suboptimal times and showed agreement with the experimental data, showing that optimal perturbation theory can describe transient growth if the initial disturbance state is known.

Descriptors: Laminar-turbulent transition, receptivity, crossflow instabilities, transient growth, Falkner-Skan-Cooke boundary layer, swept flat plates, asymptotic suction boundary layer, free-stream turbulence, surface roughness.

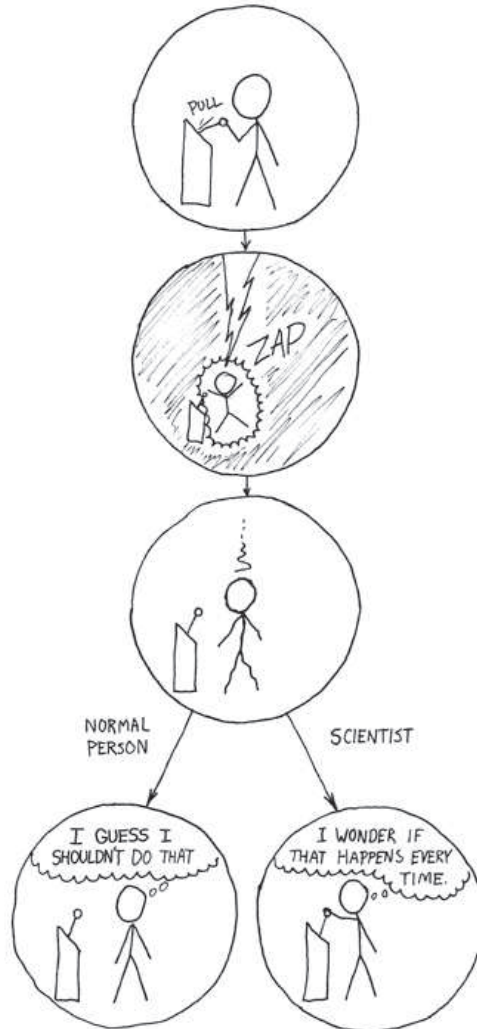
Preface

This doctoral thesis is within the area of fluid mechanics, concentrating on transition in boundary layer flow with special attention to receptivity and growth. This was studied experimentally using hot-wire anemometry in boundary layers on swept flat plates and in the asymptotic suction boundary layer. The thesis is divided into two parts, where the first part is an overview of the current understanding of transition and also summarises the present contribution to the field of fluid mechanics. The second part consists of three papers, which are adjusted to comply with the present thesis format for consistency. However, their contents have not been changed compared to published or submitted versions except for minor refinements. In chapter 6 of the first part in the thesis the respondent's contributions to all papers are stated.

May 2010, Stockholm

Thomas Kurian

The Difference



How could you choose something a little bit over-
understanding a more lightning response?

<http://xkcd.com/242>

Contents

Abstract	iii
Preface	iv
Chapter 1. Introduction	1
Chapter 2. An overview of boundary layer transition	4
2.1. Fundamentals of fluid mechanics	4
2.2. Receptivity	4
2.3. Linear theory	6
2.4. Bypass transition	8
Chapter 3. Baseflows under investigation	11
3.1. Crossflow instabilities in the Falkner-Skan-Cooke boundary layer	11
3.2. Asymptotic suction boundary layer	14
Chapter 4. Experimental techniques and set-ups	18
4.1. The MTL wind-tunnel facility	18
4.2. Measurement techniques	18
4.3. Turbulence generating grids	23
4.4. Falkner-Skan-Cooke boundary layer set-up	24
4.5. Asymptotic suction boundary layer set-up	26
Chapter 5. Results and Conclusions	28
5.1. Grid-generated turbulence	28
5.2. Crossflow instabilities	28
5.3. Asymptotic suction boundary layer	29
Chapter 6. Papers and authors contributions	30
Appendix A. Filtering of signals	32

Acknowledgements	36
References	38

Part I

Overview and summary

CHAPTER 1

Introduction

Fluid flows can be divided into two regimes, one laminar and the other turbulent. Laminar flows tend to be well-structured and predictable, while turbulent flows are characterised by chaotic motion. For an airplane wing, the state of the flow near the leading edge is laminar but further downstream it becomes unstable and susceptible to disturbances, which will grow, and eventually the flow will become turbulent. This process is called transition and is the main focus of the present work.

In certain industrial applications turbulence has some benefits. It can be used to enhance mixing of fluids, to aid in heat transfer or to prevent separation. But for most aerodynamic designs turbulence has negative connotations. For flows over turbine blades, the increased heat transfer due to turbulence can lead to fatigue and eventual failure of the material. For flows over wings, turbulence causes an increase in skin friction and thus an increase in drag and fuel consumption.

For passenger aircrafts in free-flight, this friction drag constitutes the largest part of the total drag. Of this, the friction drag on the wings represents the best opportunity for drag reduction strategies. For drag reduction design we are interested in a thin region of flow where the presence of the aerodynamic body serves to accelerate the fluid, making any fluid that actually touches the surface of the body have zero velocity, with respect to the surface. This region is called the boundary layer and is characterised by a steep velocity gradient. The velocity gradient at the wall together with the fluid's dynamic viscosity determines the amount of friction that the fluid flow exerts on the surface. Turbulent boundary layers have a much steeper gradient at the wall and thus result in a higher skin friction as compared to a laminar boundary layer. By better understanding the transition to turbulence it could be possible to design future wings to have much larger regions of laminar flow over them and thus reduce the fuel consumption of the aircraft, and thereby reduce the negative environmental impact of air travel.

A starting point for studies of laminar to turbulent transition in wall bounded flows dates back to the pipe flow experiments of Reynolds (1883). Since then a lot more has been learned about transition scenarios in a variety of flow cases. The difficulty in understanding transition has been caused in part

by the many different routes a laminar flow can take to become turbulent, but ideally the transition process can be broken down into three stages: receptivity, disturbance growth and breakdown. Receptivity refers to how external disturbances enter the boundary layer. The sources of these disturbances, to name a few, are surface roughness and free-stream turbulence. Despite being the first step in transition, receptivity has only received serious attention within the last 30 years.

The disturbance growth is the most well understood step of the transition process. For clean flow conditions, 2D disturbances grow exponentially and form what are called Tollmien-Schlichting (TS) waves. Once these disturbances reach sufficiently high amplitudes nonlinear effects start to take over and a rapid breakdown to turbulence occurs. For environments with larger external disturbances streamwise streaks develop, i.e. region of alternating low and high speed streaks, which grow algebraically. Once the amplitude of these streaks become large, the gradients in the spanwise direction give rise to secondary instabilities. These instabilities grow on the streaks and cause the development of turbulent spots which spread out and make the surrounding boundary layer turbulent as well.

To keep the flow laminar over the wing, one can either try to relaminarise the flow after it has become turbulent or try to delay the location of transition so that laminar flow covers a larger percentage of the wing. Relaminarising turbulent flow is not a pragmatic solution for airplane wings as the energy saved may be outstripped by the energy expended to achieve relaminarisation.

Transition delay can also be divided into the strategies of active and passive flow control. Active flow control attempts to delay transition by acting on the flow, for example with blowing or suction, to fight against the growth of disturbances. The asymptotic suction boundary layer (ASBL) is an example of this where the baseflow is changed to be a more stable state. TS-waves do not grow in the ASBL until high Reynolds numbers. The drawback of this is similar to the relaminarisation of a turbulent boundary layer where the energy expended may be greater than the energy saved.

Passive flow control aims to delay transition by designing a wing such that the natural route to transition is avoided. The clear advantage of passive flow control is that it requires no energy input. The drawback, however, is that once it is designed it cannot be altered for other flow conditions and a poorly designed wing with passive control can actually trigger transition through a different route. For example, a wing designed to delay transition in a high turbulence intensity environment will not prevent transition due to surface roughness in a low turbulence environment. This emphasises the importance of fully understanding the transition process in a variety of flow conditions.

Part I of this thesis serves as an introduction to this work, with Chapter 2 dealing with some basic concepts in stability and transition. Chapter 3 gives

details about the stability characteristics of the baseflows studied in this thesis followed by chapter 4 which gives details of the experimental setup. Chapter 5 summarises the key points of this work and presents conclusions. Part II consists of three papers that delve further into free-stream turbulence as a source of receptivity, the development of crossflow instabilities and the growth of disturbances in the asymptotic suction boundary layer.

CHAPTER 2

An overview of boundary layer transition

2.1. Fundamentals of fluid mechanics

Fluid flows are governed by the Navier-Stokes equations (NSE) and the continuity equation. The nondimensionalised, incompressible form of the equations are stated here in tensor notation as,

$$\frac{\partial u_i}{\partial t} + u_j \frac{\partial u_i}{\partial x_j} = -\frac{\partial p}{\partial x_i} + \frac{1}{Re} \frac{\partial^2 u_i}{\partial x_j \partial x_j} \quad (2.1)$$

$$\frac{\partial u_i}{\partial x_i} = 0, \quad (2.2)$$

where u_i is the i^{th} component of the velocity vector, p is the pressure and Re is the Reynolds number. The NSE is simply a restatement of Newton's second law of motion¹ for a fluid element, while the continuity equation is a restatement of the principle of mass conservation. Re is the most important parameter for fluid flows and gives an idea of the ratio of inertial to viscous forces. It is defined as $Re = UL/\nu$ where U is a reference velocity, L is a reference length scale and ν is the kinematic viscosity. A low Re means that viscous forces dominate over inertial forces and a high Re means the opposite. To get an idea of this, a list of the Reynolds number for familiar items is provided in table 1.

Due to the nonlinear nature of these equations, there exist no exact solutions in general. The complexity of these equations together with the problem of formulating appropriate boundary conditions limits the possibilities to obtain solutions for flows of technical interest even with the largest computers presently available.

2.2. Receptivity

Receptivity is the first stage of transition and aims to describe how disturbances enter the boundary layer. These disturbances can originate from the surface, for example due to roughness, vibrations or surface curvatures. They can also originate from the external flow in the cases of vortical or acoustic disturbances. The term was coined by Morkovin (1969) where he emphasised

¹ $F = ma$ or as it is expressed in the Navier-Stokes equations $a = F/m$.

	Re
A bacterium, swimming at 0.01 mm/s	0.00001
Dust particles in air	1
Flapping wings of the smallest flying insects	30
A dragonfly going 7 m/s	30,000
A duck flying at 20 m/s	300,000
A tuna at 10 m/s	30,000,000
The wing of a large commercial aircraft	100,000,000
A large whale swimming at 10 m/s	300,000,000
A nuclear submarine	1,000,000,000

TABLE 1. Order of magnitude estimates of the Reynolds numbers of various objects in nature and technology compiled from Vogel (1996) and Wegener (1997).

the importance of characterising the environmental disturbances of testing facilities when considering transition studies. He postulated that there must be some type of transfer function between the free-stream disturbances and the initial disturbances in the boundary layer. Once these initial disturbances are set up in the boundary layer, they will grow according to stability theory. A full review of receptivity of the boundary layer is given by Saric, Reed & Kerschen (2002) and the discussion here serves only as an overview.

Receptivity as a catch-all term belies its complexity, and in reality it is dependent of many factors. These factors include the type of disturbance, whether they be vortical disturbances, acoustic disturbances or surface roughness, the characteristics of said disturbances as well as the shape of the leading edge of the body.

The initial theoretical work on receptivity of TS-waves (discussed in the next section) was performed by Goldstein (1983, 1985). Using asymptotic analysis, he points out that a resonance is needed between the disturbances in the free stream and the most dangerous eigenmode. A scale conversion is needed to trigger TS-waves from free-stream disturbances since the disturbances in the free stream are of a much longer wavelength than the TS-wave. This scale conversion was also shown to occur in regions of sudden variations of the baseflow, such as in areas of surface non-uniformities, i.e. surface roughness and surface curvature.

Wanderley & Corke (2001) showed that the receptivity coefficients change for differences in the shape and aspect ratio of the leading edge. Not only does the shape of the leading edge affect receptivity, but also the derivative of the shape can act as a source of receptivity if it is discontinuous (cf. Saric *et al.* 2002).

Experimentally, receptivity coefficients are further complicated by the fact that they cannot be measured directly, but only inferred after the disturbances have significantly grown.

2.3. Linear theory

2.3.1. Linear growth

The linear theory is based on the decomposition of the Navier-Stokes equation into a base state and a small disturbance to this base state,

$$u_i = U_i + u'_i, \quad p = P + p'. \quad (2.3)$$

For a 2D Blasius boundary layer (BBL) the base state can be expressed as $(U_1, U_2, U_3) = (U, V, W) = (U(y), 0, 0)$. The disturbances are expressed as $(u'_1, u'_2, u'_3) = (u, v, w)$ and are assumed to be of the form

$$v(x, y, z, t) = v(y)e^{i(\alpha x + \beta z - \omega t)}, \quad (2.4)$$

where v is the wall-normal velocity, α and β refer to the streamwise and spanwise wavenumbers respectively and ω refers to the angular frequency. By eliminating the nonlinear terms in the NSE and applying the disturbance assumption, we arrive at the Orr-Sommerfeld (OS) equation

$$\left[(-i\omega + i\alpha U)(D^2 - k^2) - i\alpha U'' - \frac{1}{Re}(D^2 - k^2)^2 \right] \hat{v} = 0, \quad (2.5)$$

where $k^2 = \alpha^2 + \beta^2$ and D is d/dy . The Reynolds number is based on the displacement thickness, $Re = U\delta^*/\nu$.

To describe 3D disturbances we introduce the wall-normal vorticity, $\eta = \partial u/\partial z - \partial w/\partial x$, with the same assumption used for the wall-normal perturbation,

$$\eta(x, y, z, t) = \eta(y)e^{i(\alpha x + \beta z - \omega t)}, \quad (2.6)$$

Now the Squire equation can be derived to yield,

$$\left[(-i\omega + i\alpha U) - \frac{1}{Re}(D^2 - k^2) \right] \hat{\eta} = -i\beta U' \hat{v}. \quad (2.7)$$

which is combined with 2.5 to form the Orr-Sommerfeld-Squire (OSS) equations.

The 2D solution ($\beta = 0$) to the spatial problem (ω is real), results in complex eigenvalues for α and complex eigenfunctions for $v(y)$. This means that the disturbance is

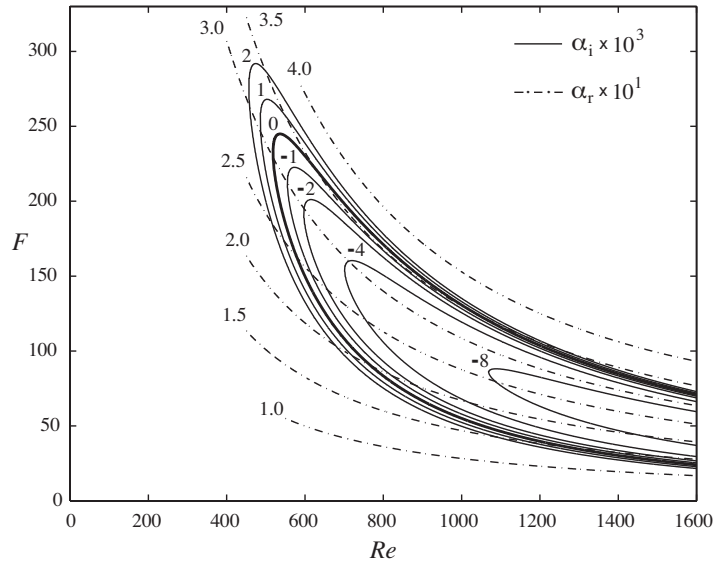


FIGURE 2.1. Solutions to the OS equation in the BBL. Solid and dash-dotted lines represent the iso-lines of imaginary and real wavenumber, respectively. The nondimensional frequency is defined as $F = (\omega\nu/U_\infty^2) \times 10^6$. The neutral stability curve is shown as the thick black line. Figure taken from Fransson & Alfredsson (2003).

$$v \propto e^{i(\alpha_r x - \omega t)} e^{-\alpha_i x}. \quad (2.8)$$

The first exponential is a sine wave that represents the well-known Tollmien-Schlichting (TS) wave, which will have a streamwise wavenumber of α_r . The second exponential determines the growth rate of the disturbance, with negative values for α_i leading to exponential growth. The total growth of a disturbance can be expressed as an N -factor,

$$N = \int_{x_0}^x \alpha_i(x) dx = \ln \left(\frac{A(x)}{A(x_0)} \right), \quad (2.9)$$

where x_0 is the location of the start of the growth and A is the amplitude of the disturbance at a certain streamwise location. What we mean by an N -factor is that at a certain location the disturbance has been amplified by a factor of e^N . This is a popular method of transition prediction, where the flow is considered turbulent after the disturbances have grown by a factor N . This value is determined empirically and varies from flow case to flow case.

Figure 2.1 shows the resulting solution to the OS equation. The neutral stability curve, where the growth rate of the TS-wave is 0, is shown as the thick black line. Inside this curve TS-waves will grow exponentially, while outside this curve they will decay exponentially. This theory was developed in the beginning of the 20th century, but due to lack of proper low turbulence intensity facilities and the difficulty of generating the initial disturbances in a controlled manner, experimental confirmation of TS-waves first came during WWII and was later published in Schubauer & Skramstad (1948).

2.3.2. *Nonlinear growth*

Once TS-waves have reached a sufficient amplitude, nonlinear effects start to emerge resulting in a three-dimensional flow that leads to the breakdown to turbulence. This breakdown can be divided into two regimes, the fundamental, also called K-type, and the subharmonic, also called N-type.

K-type transition was first noticed under controlled conditions by Klebanoff, Tidstrom & Sargent (1962), where transition was triggered by a mixture of 2D and 3D modes. The 2D TS-waves were generated by a vibrating ribbon, while the stationary 3D disturbances were generated by cellophane tape placed underneath the ribbon, leading to a spanwise dependence of the mean flow. They found that sudden spikes of low velocity appeared at the onset of breakdown and that these spikes multiplied as they convected downstream, which was attributed to secondary instabilities.

N-type transition is seen for lower levels of TS amplitudes and show the development of staggered Λ -shaped structures. Typically, this transition process is dominated by a subharmonic frequency, $f_{1/2}$, that is half that of the fundamental frequency, f_1 . Later stages of N-type transition show smooth transition to turbulence rather than a violent breakdown, with fundamental and subharmonic frequencies interacting to produce growth at higher frequencies such as, $f_{3/2}$, $f_{5/2}$. No sudden spikes are seen as in K-type transition.

Kachanov (1994) pointed out that in well-controlled experiments with disturbances generated at a single frequency neither K nor N-type transition scenarios resulted in turbulent spots as would be observed for "natural" transition where the initial forcing is much more complex. This suggests that natural breakdown is susceptible to a wide range of frequencies that have a complex interaction.

2.4. Bypass transition

2.4.1. *Transient growth*

For high levels of external disturbances, the TS-wave scenario does not accurately describe transition to turbulence. The earliest experiments looking at the effect of FST on a laminar boundary layer were performed by Klebanoff (1971). More recent investigations include those of Westin *et al.* (1994) and

Matsubara & Alfredsson (2001). They show that increasing the level of FST in the wind tunnel results in the generation of high and low speed streaks oriented in the streamwise direction. Furthermore, the amplitude of these streaks grew as they travelled downstream and transition was found to occur at subcritical Re , thus ruling out an explanation based on TS-waves. Reshotko (2001) joked that prior to the 1990's "bypass transition either bypassed the TS processes or bypassed our knowledge, or both." The theoretical foundation for this transient growth was laid by Landahl (1980), where he showed that for a small wall normal perturbation could feed energy into the streamwise component and cause significant linear growth. This was dubbed the "lift-up" mechanism and helped explain the presence of streamwise streaks.

Transient growth occurs due to the non-orthogonality of the OSS system. Even as the solution might predict exponential decay for all modes, the superposition of decaying modes might result in a region of algebraic growth followed by exponential decay. An idea to try and calculate transient growth is the concept of optimal perturbations. This refers to a method which aims to maximise the energy for a given time. One of the earliest works done on optimal perturbation was that of Butler & Farrell (1992) using a temporal framework, where they maximised the disturbances in time. This assumes a parallel flow, i.e. a spatially invariant boundary layer, to compare with transient growth in the streamwise direction. Luchini (1996, 2000) and Andersson *et al.* (1999, 2001) calculated the optimal perturbations in a spatially developing boundary layer. While a spatially invariant boundary layer would exhibit exponential viscous decay, Luchini (1996, 2000) showed that this viscous decay becomes weaker with distance in a spatially growing boundary layer and was not enough to overcome the transient growth.

Controlled experiments were performed by Westin *et al.* (1998), using local injection of a free-stream disturbance and by White (2002), White & Ergin (2003), Fransson *et al.* (2004), and White *et al.* (2005) looking at transient growth caused by surface roughness. Using a spanwise array of roughness elements the authors were able to control the spanwise wavenumbers of the disturbances. They found optimal disturbances inadequate to describe the transient growth owing to the suboptimality of the initial disturbance. Fransson *et al.* (2004) showed that introducing a suboptimal perturbation instead better described the transient growth.

2.4.2. *Secondary instabilities*

Once these streaks have reached a relatively high amplitude, they become susceptible to secondary instabilities due to the large gradients in the spanwise and wall-normal directions. Matsubara & Alfredsson (2001) showed through flow visualisations the breakdown of streaks into turbulent spots. The streaks were observed to exhibit a slight wiggle, whose amplitude increased in the downstream direction till a turbulent spot was formed. This wiggle occurred

on the low speed streak and resembled a sinuous type instability. Asai, Minagawa & Nishioka (2002) measured the sensitivity of a low speed streak to both a sinuous and varicose disturbance. They found that the varicose instability displayed higher maximum growth rates than the sinuous mode, but that the sinuous modes grew throughout the measurement domain, while the varicose mode eventually decayed.

CHAPTER 3

Baseflows under investigation

3.1. Crossflow instabilities in the Falkner-Skan-Cooke boundary layer

Three-dimensional flow such as those over swept wings, rotating cones and discs are well described by the Falkner-Skan-Cooke family of boundary layer similarity solutions (FSC). They describe flows accelerated in the streamwise direction with a constant spanwise velocity. The acceleration is assumed to follow a power law,

$$U(x) = C(x - x_0)^m, \quad (3.1)$$

where m is an acceleration parameter. The boundary layer similarity equations for the FSC are

$$f''' + ff'' + \beta_H(1 - f'^2) = 0 \quad (3.2)$$

$$g'' + fg' = 0 \quad (3.3)$$

with $U(y) = U_\infty f'(\xi)$ and $W(y) = W_\infty g(\xi)$ (Schmid & Henningson 2001). Additionally, ξ is a nondimensional wall-normal coordinate. β_H is called the Hartree parameter and it is related to the acceleration parameter as,

$$\beta_H = \frac{2m}{1+m} \quad \text{or} \quad m = \frac{\beta_H}{2 - \beta_H}. \quad (3.4)$$

3.1.1. Linear theory

The linear stability equations can be derived for the FSC in the same manner as the BBL, but with a baseflow of $(U, V, W) = (U(y), 0, W(y))$, which leads to the following OSS system,

$$\left[(-i\omega + i\alpha U + \mathbf{i}\beta\mathbf{W})(D^2 - k^2) - i\alpha U'' - \mathbf{i}\beta\mathbf{W}'' - \frac{1}{Re}(D^2 - k^2)^2 \right] \hat{v} = 0 \quad (3.5)$$

$$\left[(-i\omega + i\alpha U + \mathbf{i}\beta\mathbf{W}) - \frac{1}{Re}(D^2 - k^2) \right] \hat{\eta} = (\mathbf{i}\alpha\mathbf{W}' - i\beta U')\hat{v}. \quad (3.6)$$

The terms in bold are the additional terms as compared to the the BBL case. The local sweep angle can be calculated as $\alpha_s = \tan^{-1}(W/U)$.

3.1.2. Receptivity and disturbance growth

Significant experimental work has been done on the growth of disturbances in the FSC over the last 25 years, and some of the results will be discussed here. For a more complete review the interested reader is referred to Bippes (1999) for a review of experiments for swept wing flow and to Saric, Reed & White (2003) for a more general review of transition in 3D boundary layers.

Crossflow instabilities are different from TS-waves in that they can be either stationary or travelling. The travelling modes have a higher growth rate according to linear theory, but in most experiments and in free-flight condition, transition has been usually dominated by stationary disturbances. The earliest experiments on swept flat plates, performed at ASU by Saric & Yeates (1985), found the emergence of the stationary mode which is seen as a spanwise variation with a fixed wavelength of the velocity signal. Building on this Radeztsky *et al.* (1994) and Reibert *et al.* (1996) used micron sized roughness with discrete spacings to trigger stationary modes at certain wavelengths and follow the development of individual modes. They found that when they set the stationary modes with a certain wavenumber, this fundamental mode was triggered along with up to nine harmonics. The experiments performed at DLR (Müller 1990; Bippes, Müller & Wagner 1991; Deyhle, Höhler & Bippes 1993), however, found both the stationary and travelling mode. Both types of modes initially grew linearly, but saturated quickly when nonlinear effects started to set in. Both groups of researchers agreed that linear theory could be used to describe the disturbance structure, but that it overpredicts the growth rate. A wide variety of linear calculations were performed and they all predicted faster growth than the experiments showed. Non-linear PSE was better able to capture the development of the disturbances up to and including saturation (Reibert *et al.* 1996), thus emphasising the importance of nonlinear effects.

The experiments at DLR were conducted on a single swept flat plate model in three different test facilities with varying free-stream turbulence intensities. The general trend was that increasing the turbulence intensities increased the amplitude of the travelling mode and decreased that of the stationary mode.

Furthermore, the saturation level of the stationary modes decrease for increasing turbulence intensity, which eventually leads to transition dominated by the travelling mode. For the highest turbulence intensity level, the stationary mode actually decayed (Bippes & Lerche 1997).

Finally, Radeztsky *et al.* (1999) forced the boundary layer with roughness and sound. They showed that there was no change to the transition location even for high acoustic levels (95 dB) over a wide range of frequencies. Thus, the travelling modes are insensitive to acoustic disturbances and are triggered by the vortical disturbances from free-stream turbulence. All this emphasises the critical role receptivity plays in crossflow dominated transition, where a slight change in the environment causes a different transition scenario.

The receptivity of swept wing flow to stationary disturbances has been studied using Finite Reynolds Number Theory (FRNT) along with direct numerical simulations (DNS) and parabolised stability equations (PSE) (see e.g. references in Ng & Crouch 1999). FRNT has produced results that match well with DNS, PSE and experiments, even while neglecting surface curvature and non-parallel effects. Bertolotti (2000) and Collis & Lele (1999) extended the FRNT to include surface curvature and non-parallel effects. They found that these effects compete with each other, with surface curvature increasing receptivity and non-parallel flow decreasing receptivity.

More recently, receptivity studies have been performed using DNS by Schrader, Brandt & Henningson (2009), and PSE by Tempelmann, Hanifi & Henningson (2010) looking at both travelling and stationary modes. Their work confirms the earlier results when pertaining to receptivity of stationary modes. They also find that the receptivity to free-stream vortical modes are related entirely to the non-parallel effects of the baseflow, which provide the scale conversion as laid out in the work of Goldstein (1985). No transient growth was found as the inflectional instability is strong in 3D boundary layers and the favourable pressure gradient reduces transient effects. The vortical modes can also interact with the surface roughness in order to generate the travelling modes, but this process is much less efficient and they conclude that the direct triggering mechanism is the one that is seen in environments with low disturbances, with respect to both free-stream turbulence and surface roughness. The authors also estimate that the stationary mode will dominate for a roughness height that is 2.5% of δ^* until the turbulence intensity reaches 0.5%. This is a much higher threshold than that found by Bippes & Lerche (1997) and Kurian, Fransson & Alfredsson (2010), *Paper 2 of the present thesis*, but can be explained as the experimental setups did not force the stationary mode with artificial roughness and thus the polished plates give a much lower value of the surface roughness height.

3.1.3. Secondary instabilities

Secondary instabilities in swept wing flow has been studied by Kawakami *et al.* (1999); Chernoray *et al.* (2005); White & Saric (2005). Numerical studies include the work of Malik *et al.* (1994, 1999) and Högberg & Henningson (1998). There is general agreement among the investigators that there exist two secondary instability modes, which include a low frequency mode located in the lower part of the boundary layer and a high frequency mode located in the upper part. We shall follow the convention of White & Saric and refer to them as Type-I for the low frequency mode and type-II for the high frequency modes. Type-I is driven by spanwise gradients in the streamwise velocity and resembles a sinuous mode, while type-II is driven by wall-normal gradients and resembles a varicose mode.

Researchers have differed on which mode is more important for transition as results have varied. The early work suggested that type-II was the most important for transition as it was noticed to occur more often. Högberg & Henningson (1998) had transition dominated by type-II but noted that type-I also exhibited growth. They refined the understanding of the transition process by stating that the flow quality most likely determined which mode dominates, with low turbulence levels favouring type-II and high turbulence level environments favouring type-I. However, the more recent work of Chernoray *et al.* (2005) and White & Saric (2005) found that type-I occurred more frequently, had higher growth rates and lead to transition. White & Saric note that the type-II mode was difficult to measure since the amplitude of the type-I mode dominated over it except in one case, which had low spanwise shear. In that case the type-II played a much more important role in transition. The final breakdown procedure is most likely a mixture of these effects, with the gradients selecting the type of mode and the turbulence level in the environment acting as a source of receptivity.

3.2. Asymptotic suction boundary layer

The asymptotic suction boundary layer (ASBL) is achieved when uniform suction is applied through the surface of a flat plate. For a fully-developed ASBL the mass flow through the wall compensates for the growth of the boundary layer and results in a spatially invariant flow, with the boundary layer thickness being constant. The ASBL has an exact solution that can be derived from the NSE. By first assuming a spatially invariant 2D flow, $\partial/\partial x = \partial/\partial z = 0$, the continuity equation becomes,

$$\frac{\partial v}{\partial y} = 0. \quad (3.7)$$

Thus the wall-normal velocity, $v = V_0$, throughout the boundary layer, where V_0 is the suction velocity. For convenience V_0 will be given as positive in

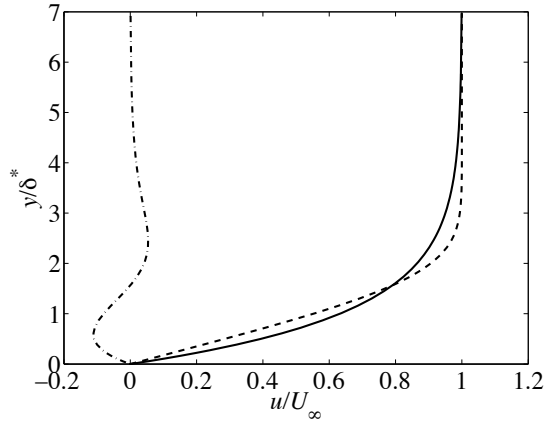


FIGURE 3.1. Boundary layer profiles of the BBL (---), the ASBL (—) and their difference (- · -).

the direction of suction. By now solving for a steady flow with zero pressure gradient, the momentum equation for the streamwise velocity becomes

$$-V_0 \frac{\partial u}{\partial y} = \nu \frac{\partial^2 u}{\partial y^2} \quad (3.8)$$

with boundary conditions $u(0) = 0$ and $u(\infty) = U_\infty$. This equation can be solved exactly to yield

$$\frac{u}{U_\infty} = 1 - e^{-yV_0/\nu}. \quad (3.9)$$

The base flow is shown in figure 3.1 along with the BBL for comparison. Integration of the boundary layer to obtain the displacement thickness, δ^* , and momentum-loss thickness, θ , yields

$$\delta^* = \frac{\nu}{V_0}, \quad \text{and} \quad \theta = \frac{1}{2} \frac{\nu}{V_0}. \quad (3.10)$$

The shape factor, $H_{12} = 2$ and the Reynolds number based on the displacement thickness is

$$Re = \frac{U_\infty}{V_0}. \quad (3.11)$$

One advantage of the ASBL is that Re is decoupled from the Reynolds number based on streamwise distance, thus allowing us to vary these parameters independently.

3.2.1. *Linear theory*

Applying linear stability theory to this baseflow, $(U, V, W) = (1 - e^{-yV_0/\nu}, -V_0, 0)$, results in the following OSS system

$$\left[\left(-i\omega + i\alpha U - \frac{\mathbf{1}}{\mathbf{Re}} \mathbf{D} \right) (D^2 - k^2) - i\alpha U'' - \frac{1}{Re} (D^2 - k^2)^2 \right] \hat{v} = 0 \quad (3.12)$$

$$\left[\left(-i\omega + i\alpha U - \frac{\mathbf{1}}{\mathbf{Re}} \mathbf{D} \right) - \frac{1}{Re} (D^2 - k^2) \right] \hat{\eta} = -i\beta U' \hat{v} \quad (3.13)$$

with the terms in bold representing the difference between the BBL.

The OS equation for the ASBL was first solved by Hocking (1975) where he found a critical Reynolds number of 54370. Thus TS-waves will grow only for flows with relatively low levels of suction.

Experiments in the ASBL are rare due the difficulty in building the experimental setup. Some experimental work has been performed, but were focused mainly on the determination of the baseflow (Schlichting 1979, and references contained therein).

Fransson & Alfredsson (2003) investigated the development of TS-waves in the ASBL at a low Re and found that they decayed although at a slower rate than predicted by linear theory. Several possibilities for this discrepancy were offered including a small pressure gradient, noise contamination, potential 3D disturbances caused by oblique modes and the change in the baseflow over the non-porous section of the plate where the TS-waves were generated.

3.2.2. *Disturbance growth*

Experimentally, Fransson & Alfredsson (2003) also studied the development of the ASBL under vortical disturbances caused by free-stream turbulence. They found that in contrast to the BBL where the amplitude of the disturbances grew, the disturbance level in the ASBL remained nearly constant throughout the measurement regime. The value of this constant disturbance level seemed linearly related to the turbulence intensity. Furthermore, the spanwise streak spacing remained the same as the BBL case, but when suction was applied it had the effect of compressing the streaks so that they appeared flatter.

Yoshioka, Fransson & Alfredsson (2004) extended the parameter range of Fransson & Alfredsson (2003) and found that for increasing suction the disturbance level actually decayed. They also showed that the disturbance growth was not well described by optimal perturbation theory owing most likely to the nonoptimality of the generated disturbances.

Bypass transition was investigated with optimal perturbation theory in the temporal framework by Fransson & Corbett (2003), where they found good agreement with the experiments of Fransson & Alfredsson (2003), provided that

the optimal perturbation matched the streak spacing in the experiments. The experiments, however, did not match the global optimal, but since the streamwise spacing was dependent on the turbulence intensity level it was thought that increasing this level would eventually reconcile the difference between the experiments and the theory. Byström, Levin & Henningson (2007) studied the ASBL with optimal perturbation theory in a spatial framework and found the same global optimal perturbation but with a 16% larger growth than the temporal framework.

The focus of Kurian & Fransson (2010), *Paper 3 in the present thesis* is to have a more controlled study of the optimal perturbation theory as it pertains to experiments by a parametric investigation performed using an array of cylindrical roughness elements. These elements were placed on the surface with a spanwise spacing corresponding to the optimal perturbation. Different roughness heights were tested and the results were compared to optimal perturbation theory.

Experimental techniques and set-ups

4.1. The MTL wind-tunnel facility

The minimum-turbulence-level (MTL) wind-tunnel facility is a closed-loop, temperature-controlled wind tunnel, which as its name implies has a very clean base flow. The test section is 7 m long with a cross section of 1.2 m in width and 0.8 m in height. A sketch of the wind tunnel is shown in figure 4.1. The flow quality was checked and after 10 years of operation reconfirmed to have a streamwise fluctuation level of 0.025% in the streamwise direction and 0.035% in the spanwise and wall-normal direction (Lindgren & Johansson 2002) at $U_\infty = 25 \text{ ms}^{-1}$. This is achieved by a good aerodynamic design of the full flow loop as well as a series of honeycombs and turbulence reducing meshes in the stagnation chamber and a high contraction ratio (9:1) leading into the test section.

A heat exchanger is located after the fan and before the first corner. This along with a thermocouple at the end of the test section forms a feedback loop that can maintain a constant temperature in the wind tunnel to within $\pm 0.05^\circ\text{C}$. This serves as a great advantage for hot-wire measurements where a fluctuation in temperature needs to be accounted for to give an accurate velocity (discussed in the next section)

A computer-controlled five-axis traversing system allows for measurements in the x - y - z coordinate system. Additional axes in yaw and roll allow for *in situ* automatic angular calibration for X- and V-probes.

Signals are recorded using Labview with a 16-bit NI PCI-6040E data acquisition card. All these features combine to facilitate the execution of lengthy experiments (in this study up to 30 hours) run entirely automatically.

4.2. Measurement techniques

The velocity measurements in this thesis were performed using hot-wire anemometry. The advantage of this method is that it provides a small localised flow velocity with high temporal resolution. Hot-wires are made of a thin, 1-5 μm , wire, usually platinum or tungsten, soldered or welded between two prongs. The probe is connected as one of the arms in a Wheatstone bridge, where a current is passed through it, which heats the wire. By selecting the resistance

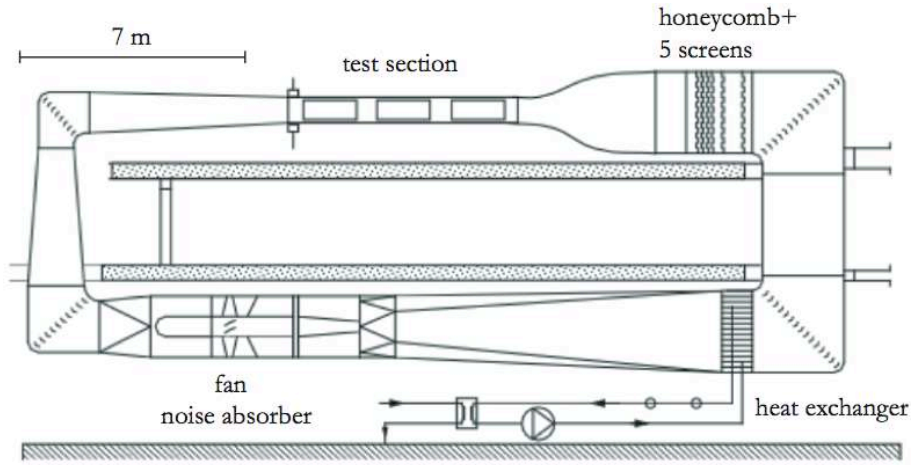


FIGURE 4.1. Sketch of the MTL wind tunnel.

of the other arm in the bridge, the level of current can be adjusted. The Wheatstone bridge is connected to a servo-amplifier, which works to keep the resistance and thus the temperature of the hot-wire constant. When placed in a fluid flow the wire is cooled due to forced convection. To ensure that the forced convection is the dominant cooling source, the length to diameter ratio of the wire should be greater than 200. Once the heat transfer from the wire is assumed to be entirely forced convection, a relation between the voltage needed to maintain the hot-wire at constant temperature, E , and the fluid velocity, U_{eff} , is given by King's Law

$$E^2 = A + BU_{eff}^n, \quad (4.1)$$

where A , B , and n are constants determined by calibration. The U_{eff} here is the effective cooling velocity, which is the velocity of the component normal to the wire. There is a small component of heat transfer that runs parallel with the wire but this is small compared to the heat transfer from the flow normal to it.

The voltage given by the anemometer is affected not only by the forced convection, but also the temperature changes of the surroundings. A temperature correction can be applied to the voltage

$$E(T_{ref})^2 = E(T)^2 \left(1 - \frac{T - T_{ref}}{OH/\alpha_{el}} \right)^{-1}, \quad (4.2)$$

where α_{el} is the resistive temperature coefficient of the wire and OH is the overheat ratio defined $(R_h - R_c)/R_c$, where R_h and R_c are the resistances of

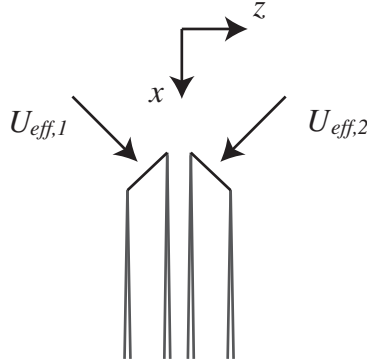


FIGURE 4.2. Sketch of a V-probe with the resulting effective cooling velocities.

the hot-wire with and without current passing through it, respectively. For the MTL tunnel, $T = T_{ref}$, so this temperature correction is not needed.

For cases where low velocities need to be measured, for example near the wall, an additional term is added to account for the free convection that will occur (Johansson & Alfredsson 1982). Called Modified King's Law, the relation is

$$U = k_1(E^2 - E_0^2)^{1/n} + k_2(E - E_0)^{1/2}, \quad (4.3)$$

where E_0 is the voltage at zero velocity and k_1 , k_2 and n are calibration constants.

A single hot-wire can measure the flow velocity in only one direction. To be able to measure in two directions, we can use a dual-sensor probe such as an X- or V-probe. These probes have two sensors set at an angle to each other, see figure 4.2. Since each wire can only measure the velocity normal to it, each sensor will record a different value. By adding the components from each sensor together, the streamwise velocity, U , can be extracted and similarly by subtracting the components, the spanwise velocity, W , can be extracted. X-probes are built with one wire offset above the other. When viewed from upstream the prongs form the corners of a square, thus the sensor averages the flow over a 3D measurement volume. V-probes are built with the wires in the same plane as shown in figure 4.2, i.e. the four prongs are in a straight line. X-probes are used in a spatially homogeneous flow, i.e. the free stream, whereas the V-probes are used in the boundary layer, where the strong wall-normal gradients present a challenge to measuring with an X-probe.

The probe is calibrated by yawing it at several different angles at several speeds. Figure 4.3 shows a resulting calibration profiles done at nine angles

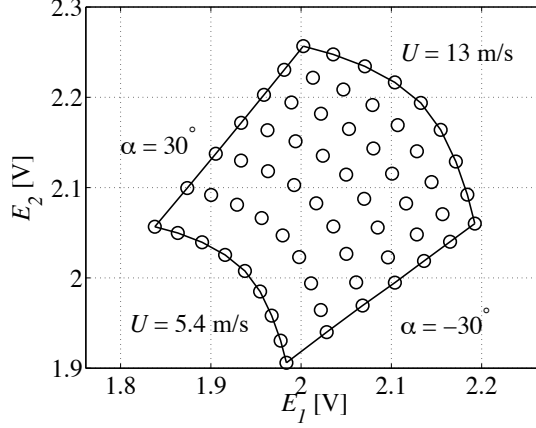


FIGURE 4.3. Typical angular calibration for a dual-sensor probe.

between -30° and 30° and seven speeds between 5.4 m s^{-1} and 13 m s^{-1} . The variables $x = E_1 + E_2$ and $y = E_1 - E_2$ are then calculated and fitted to a 2-dimensional fifth order polynomial,

$$\begin{aligned}
 U = & a_{0,0} + a_{1,0}x + a_{2,0}y + \\
 & a_{3,0}x^2 + a_{4,0}xy + a_{5,0}y^2 + \\
 & a_{6,0}x^3 + a_{7,0}x^2y + a_{8,0}xy^2 + a_{9,0}y^3 + \\
 & a_{10,0}x^4 + a_{11,0}x^3y + a_{12,0}x^2y^2 + a_{13,0}xy^3 + a_{14,0}y^4 + \\
 & a_{15,0}x^5 + a_{16,0}x^4y + a_{17,0}x^3y^2 + a_{18,0}x^2y^3 + a_{19,0}xy^4 + a_{20,0}y^5, \\
 \tan\alpha = & a_{0,1} + a_{1,1}x + a_{2,1}y + \\
 & a_{3,1}x^2 + a_{4,1}xy + a_{5,1}y^2 + \\
 & a_{6,1}x^3 + a_{7,1}x^2y + a_{8,1}xy^2 + a_{9,1}y^3 + \\
 & a_{10,1}x^4 + a_{11,1}x^3y + a_{12,1}x^2y^2 + a_{13,1}xy^3 + a_{14,1}y^4 + \\
 & a_{15,1}x^5 + a_{16,1}x^4y + a_{17,1}x^3y^2 + a_{18,1}x^2y^3 + a_{19,1}xy^4 + a_{20,1}y^5,
 \end{aligned} \tag{4.4}$$

with $\alpha = W/U$ (Österlund 1999). The coefficients a_{ij} are fitted using a least squares minimization.

To be able to measure the V -component in the free stream, a second X-probe was set up and calibrated in the same way and afterwards rotated 90° . To accurately rotate the probes, two holders were manufactured with slots at 90° intervals and two probe supports with a placement pin. After calibration one of the probes was unlocked from the probe support and rotated to fit the

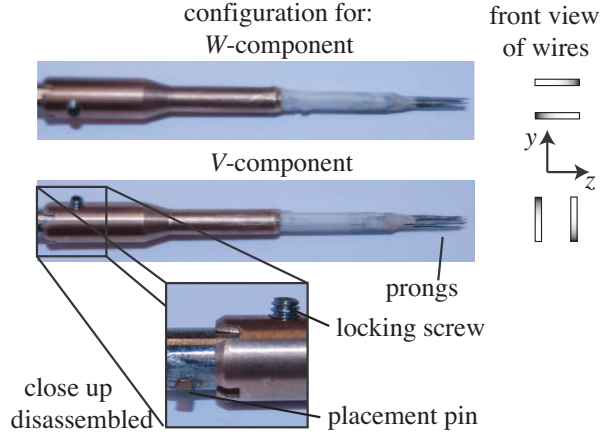


FIGURE 4.4. Photograph of the X-probes used in the experiments shown in the two configurations for measuring the W and V component.

adjacent slot into the placement pin. The configurations are shown in figure 4.4.

As stated earlier, a disadvantage of using dual-sensor probes is that they cannot be used in flows with sharp gradients over the two sensors. The calibration of these probes assumes homogeneous flow in the measurement volume. However, if one sensor is in a region of high speed flow, while the other is in lower speed flow, the superposition and difference of the signals will result in an artificial velocity. To correct for this Cutler & Bradshaw (1991) proposed a solution where the gradient in the flow is taken into account. This is given by

$$u = u_m + \frac{\Delta}{2} \frac{\partial w_m}{\partial z} \quad (4.5)$$

$$w = w_m + \frac{\Delta}{2} \frac{\partial u_m}{\partial z}, \quad (4.6)$$

where u and w refer to the true velocities and the subscript m refers to the measured velocities. Δ is the spacing between the wires. This solution can only correct for the mean velocity signal and not the time-dependent velocity signal as the time-dependent spanwise variation is not known. In the experiments in this thesis only a spanwise gradient needed to be accounted for so only the relevant components are mentioned. Those interested in the full correction for complex 3D flows are referred to Cutler & Bradshaw (1991).

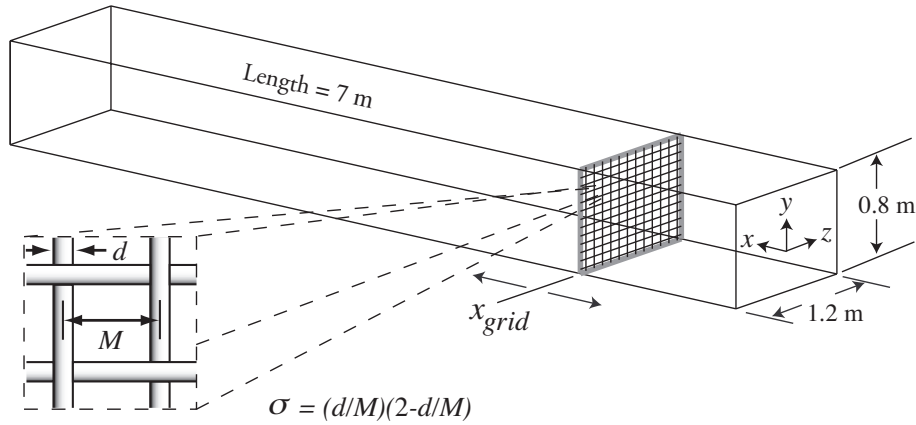


FIGURE 4.5. Sketch of a grid in the wind tunnel.

4.3. Turbulence generating grids

For the study on receptivity to free-stream turbulence (FST), it was necessary to be able to vary the intensity and the characteristic length scales of the FST at the leading edge. This could be accomplished by the use of different turbulence-generating grids with a variation in the mesh and bar width. Five different grids of interwoven round rods with small mesh widths, ranging from 0.96 mm to 4.2 mm, were set up at the entry to the test section, see figure 4.5. The mesh-width, M , is measured from the centre of one bar to the centre of an adjacent one. The solidity of the grid, σ , is a measure of the amount of area that the grids take up compared to an empty test section (see formula in figure). The moniker LT refers to **Low Turbulence**, as these grids produce much lower levels of turbulence intensity than grids previously studied at KTH. The grids were chosen so as to maintain a solidity of approximately 0.4. This is done so that the jets emanating from the open areas of the grid are stable and do not merge, which would cause inhomogeneities in the mean flow that persist far downstream.

Since the grids were fairly flexible, they were welded to a primary frame, which served as a support. This primary frame was then fastened to a secondary frame which was press-fit into the tunnel. An advantage to this additional frame was that it could be easily set up at any streamwise position without needing to drill new holes into the test section walls. Thus we could set up the grid at a relative distance to the leading edge based on the desired parameters of turbulence intensity and integral length scales.

The flow downstream of the grids was measured with two X-probes, one to give the u and w components and the other to give the u and v components. A full description of the turbulence intensity levels, characteristic length scales,

spectra and other pertinent information is given in Kurian & Fransson (2009), *Paper 1 of the present thesis*.

4.4. Falkner-Skan-Cooke boundary layer set-up

The most important parameters determining the development of cross flow instabilities are the sweep angle of the plate, the Hartree parameter and the Reynolds number of the flow (section 3.1). Ideally the value of these parameters should be large, which would in turn give disturbance amplitudes easy to measure. However, in an experiment we have to weigh such factors against the limits of manufacturability and measurability. The first challenge is the leading edge, which was CNC¹-machined out of one solid piece of aluminum. A larger sweep angle means a longer plate, which necessitates a larger CNC-machine. The Hartree parameter together with the inlet velocity to the test section of the wind tunnel, U_0 , sets the velocity distribution and the boundary layer thickness along the plate. On one hand, large β_H and U_0 trigger large crossflow instabilities, but thin boundary layers. On the other hand, if we wish to resolve the disturbances in the boundary layer it is always preferred to have a thick boundary layer. Furthermore, a thick boundary layer would allow us to choose parameters that would ease the manufacturing of certain experimental components, such as the hot-wires and roughness elements. Taking into account these considerations local linear stability theory calculations were performed to determine appropriate parameters. The conclusion was that a sweep angle of 25° and a Hartree parameter of 0.15 would be sufficient to see N -factors of between 1.5 and 3, while still leaving a boundary layer thick enough to comfortably measure in.

Displacement bodies were designed for the ceiling and walls in order to generate the FSC boundary layer. A displacement body on the ceiling provides the needed acceleration to the flow, while displacement bodies on the walls direct the flow to more closely follow the streamlines of an infinite swept flat plate. The shape of the ceiling displacement body was determined assuming inviscid flow and incompressible mass conservation,

$$A_0 U_0 = A(x) U(x), \quad (4.7)$$

where A is the cross sectional area of the wind tunnel, U is the velocity and the subscript 0 denotes a reference position. Combining this with equations 3.1 and 3.4 results in the a shape of the ceiling displacement body as

$$A(x) = \frac{A_0 U_0}{C(x - x_0)^m}. \quad (4.8)$$

To simulate an infinitely wide swept flat plate in the wind tunnel, we would need side displacement bodies that become increasingly thicker on one

¹Computer Numerical Control



FIGURE 4.6. Photo of the completed setup in the test section. The plate is in the centre with the displacement bodies on the ceiling and walls in black. The object above the plate and reflected in the plate surface is the traversing mechanism moved far downstream.

wall and thinner on the other wall. These walls would interfere with the normal operation of the tunnel traversing system so a compromise had to be struck between good flow quality and proper operation of the wind tunnel. Once the ceiling bump was designed, inviscid CFD simulations were performed to determine the resulting streamlines for various configurations of the shape of the wall displacement bodies.

Styrofoam insulation was used to make the displacement bodies as it was easy to shape and cut out. One of the properties of styrofoam is that it melts when heated. By passing a current through a thin metal wire, thus heating it, it was possible to cut out curvilinear shapes in the styrofoam. First, the profile of the desired shape was cut out of two pieces of plywood to serve as a frame for the styrofoam. The styrofoam block was then placed between the plywood and the heated wire was dragged along the profile cutting out the desired shape. For the ceiling displacement bodies, the plywood frames were offset from each other to match the sweep angle of 25° . The styrofoam was then lightly sanded to smooth out any gouges and painted to prevent any dust from contaminating the tunnel. The displacement bodies were attached to the ceiling and walls using brass holders that were screwed into the test section. The completed experimental setup is shown in figure 4.6.

The purpose of this experiment was to study the receptivity of crossflow instabilities to both travelling and stationary disturbances. The grids described in the previous section were used to trigger the travelling modes. They were placed 1.66 m upstream of the leading edge centreline.

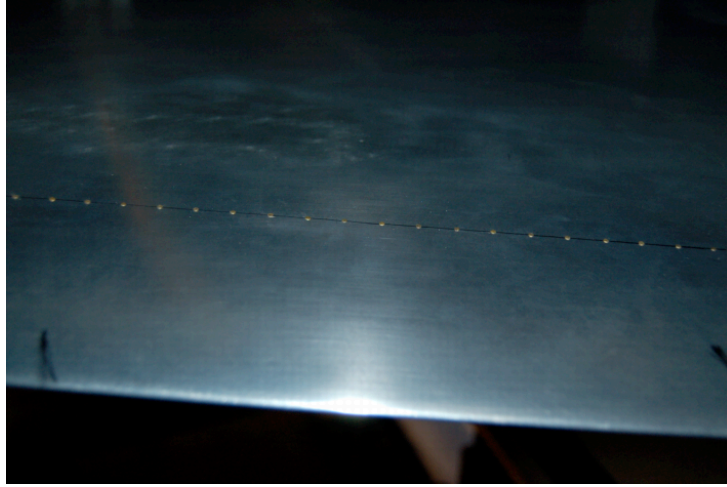


FIGURE 4.7. Photo of the roughness elements near the leading edge.

Boundary layer measurements for the travelling crossflow modes were performed using a single-sensor hot-wire. Since there is no information of the instantaneous spanwise variation of the flow, the correction of Cutler & Bradshaw (1991) cannot be used.

To trigger the stationary modes, a spanwise array of roughness elements were placed near the leading edge at $x = 91$ mm. The roughness elements were made of small cylinders 2 mm in diameter that were stamped out of thin brass plates. Two heights of roughness elements, $k = 0.22, 0.42$ mm, were placed with a spanwise spacing of $\lambda = 14$ mm. The roughness array spanned one third of the width of the leading edge. A picture of this is shown in figure 4.7.

Boundary layer measurements were performed here using a V-probe to measure the streamwise and spanwise components and the correction of Cutler & Bradshaw (1991) was used.

4.5. Asymptotic suction boundary layer set-up

The ASBL is formed when uniform suction is applied at the surface of a permeable plate. Here the permeable plate was achieved by gluing a sintered plastic porous material over a flat plate of sandwich construction. The porous material had a pore size $16 \mu\text{m}$ and a standard deviation of the roughness of $0.38 \mu\text{m}$. A sketch of the porous plate is shown in figure 4.8. The entire plate is 5.71 m long with a solid leading edge. The porous material starts at a distance of 360 mm from the leading edge and extends for 2250 mm. Suction was applied by the use of a centrifugal pump placed outside the wind tunnel connected to a pressure

Results and Conclusions

This section summarises the the main results and conclusions of the papers in the following section. For full results, the reader is referred to the appropriate papers.

5.1. Grid-generated turbulence

- Five grids giving low turbulence intensity levels, Tu , were chosen in order to generate free-stream turbulence for a future receptivity study. Two X-wires were used to measure all three velocity components as well as correlation functions. The integral, Taylor and Kolmogorov length scales were all measured independently.
- Anisotropy levels and decay rates were seen to approach the theoretical values of 1 and -1, respectively for high Reynolds numbers based on the mesh width, Re_M .
- Dissipation calculated using an assumption of isotropy and Taylor's hypothesis can give an error of as much as 50% as compared with that obtained from the downstream decay of the turbulent kinetic energy.
- Turbulent spectra showed the -5/3 decay only for high Re_M .
- A contraction was found to only have an effect on large length scales.

5.2. Crossflow instabilities

- Hot-wire measurement were performed over a swept flat plate with a pressure gradient to simulate the FSC. Travelling disturbances were triggered by using FST generated by grids located upstream of the leading edge. Stationary disturbances were triggered by a spanwise array of cylindrical roughness elements.
- Travelling modes were found for all levels of Tu tested. The initial growth was linear, followed by nonlinear behaviour, which appeared further upstream for increasing Tu . Receptivity was found to be linear throughout the range of Tu -levels measured.
- Two single hot-wires were used to determine the spanwise scale of the disturbances. It was found to be constant for high enough Tu .
- Roughness elements with small heights produced no noticeable stationary modes. Large roughness heights triggered the stationary disturbances, which were seen to follow the external streamlines. The receptivity

of the stationary modes to surface roughness is nonlinear ($E \propto Re_k^2$) for high Re_k .

- For low FST levels the stationary mode dominates over the travelling mode, whereas the opposite is true for high FST levels. There exists a threshold of $Tu = 0.25\%$ above which the stationary mode does not grow.

5.3. Asymptotic suction boundary layer

- Stationary disturbances are triggered by a spanwise array of cylindrical roughness elements in a fully developed ASBL. Hot-measurements are taken in the boundary layer at the wall-normal position that corresponds to the disturbance peak. The velocity is decomposed using a spatial Fourier transform to study the growth of individual modes.
- The fundamental mode, β_1 , along with 2 harmonics, β_4 and β_5 are seen to undergo transient growth behind the roughness elements and finally decay exponentially. For high Re_k some growth was seen in mode β_3 , suggesting that there exists a threshold below which transient growth will not occur. The location of the peak energy is seen to move further upstream for higher harmonics. The location of a peak for an individual mode moves downstream for increasing U_∞ , but remains unchanged for increasing roughness height. The receptivity is highly nonlinear with the energies scaling with factors of Re_k between $Re_k^{3.7}$ and $Re_k^{5.5}$.
- Calculations using optimal perturbation theory were performed to compare with the experimental data. The global optimal did not describe the energy growth in the experiments well. A tuning was performed to find a suboptimal time that produced a good overall result with the data. This emphasises the importance of knowing the initial state created by the roughness element as an input to the optimal perturbation calculations.

CHAPTER 6

Papers and authors contributions

Paper 1

Grid-generated turbulence revisited.

T. Kurian (TK) & J. H. M. Fransson (JF). 2009 *Fluid Dyn. Res.* **41**, 021403. It has been recompiled here in the MechThesis format with minor typographical errors corrected.

This work was of an experimental nature characterising the flow behind different turbulence generating grids. The experiments were set up and performed by TK under the supervision of JF. Data evaluation was performed by TK and the manuscript was written by JF in cooperation with TK. Parts of this work was presented at:

New results on grid-generated turbulence

T. Kurian & J. H. M. Fransson

12th EUROMECH European Turbulence Conference

September 7-10, 2009, Marburg, Germany.

Paper 2

Receptivity of crossflow instabilities to free-stream turbulence and surface roughness.

T. Kurian, J. H. M. Fransson & P. H. Alfredsson (HAL).

This work was of an experimental nature looking at the receptivity and growth of crossflow disturbances subjected independently to free-stream turbulence and surface roughness in the Falkner-Skan-Cooke boundary layer. The experimental setup was built by TK with guidance from JF. Data analysis was performed and the manuscript written by TK with input from JF and HAL. Parts of this work have been presented at:

Crossflow instabilities over a swept wing

T. Kurian & J. H. M. Fransson

7th EUROMECH Fluid Mechanics Conference

September 14-18, 2008, Manchester, United Kingdom.

and accepted for publication in:

Evolution of travelling crossflow modes over a swept flat plate

T. Kurian, J. H. M. Fransson & P.H. Alfredsson

Proceedings of the Seventh IUTAM Symposium on Laminar-Turbulent Transition

June 23-26, 2009, Stockholm, Sweden.

Paper 3

Transient growth in the asymptotic suction boundary layer.

T. Kurian & J. H. M. Fransson.

The experiments and data analysis were performed by TK. The manuscript was written by TK with input from JF. Parts of this work have been presented at:

Transient growth in the asymptotic suction boundary layer

T. Kurian

Swedish Mechanics Days 2007

June 13-15, 2007, Luleå, Sweden.

Transient growth in the asymptotic suction boundary layer

T. Kurian & J. H. M. Fransson

60th Annual Meeting of the Division of Fluid Dynamics

November 18-20, 2007, Salt Lake City, Utah, USA.

APPENDIX A

Filtering of signals

During the course of the measurements for the travelling crossflow mode, a low frequency wave was seen to dominate the time signal. Initially, this was thought to be the travelling mode, but further analysis revealed the likely presence of a spurious mode due to vibration of the arm of the traversing mechanism. Such problems were also encountered in the DLR experiments (Deyhle 1993). In this section, we shall show that this peak is the result of vibrations of the traversing arm and not related to the physics of the fluid flow. We shall further give the correction method and present the corrected data.

An energy spectrum is shown in figure A.1 for the LT_1 case at a streamwise position of 550 mm and at a wall-normal location 0.8 mm. A clear peak can be seen in the spectra at 13 Hz.

Figure A.2(a) shows the variation in the energy at 13 Hz through the boundary layer. It shows that the energy continues to increase as the probe approaches the wall. Initially this was thought to mean that the energy peak had not been resolved, and we did not traverse close to the wall for fear of breaking the hot-wire probe. The streamwise dependence of this energy peak at $y/\delta_1 \approx 1$ is shown in figure A.2(b), where the energy remains constant in the downstream direction as well. If this were energy were due to the flow physics, we would expect some growth or decay in the energy, but this is not seen. Thus we concluded that this energy peak is due to the vibration of the traversing arm and should be filtered out.

Filtering was applied by taking the energy content in a certain band, f_{band} , which corresponds to the frequencies to be filtered out, and setting them to be linearly interpolated between the values at the end of the bands. This formula is

$$p(f_{band}) = \frac{p(f_{band}(b)) - p(f_{band}(a))}{f_{band}(b) - f_{band}(a)} f_{band}, \quad (\text{A.1})$$

where a and b correspond to the start and end of the filter frequencies and p is the power spectral density. Several different bandwidths were tested and are shown in table 1. The resulting spectra are shown in figure A.3(a). For a too narrow bandwidth, the energy in the vibration is not fully filtered out. For a too wide bandwidth, the filtering starts to remove energy in frequencies

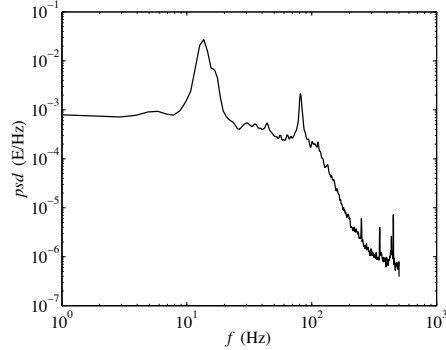


FIGURE A.1. Energy spectrum for the streamwise velocity for LT_1 at $x = 550$ mm and $y = 0.8$ mm.

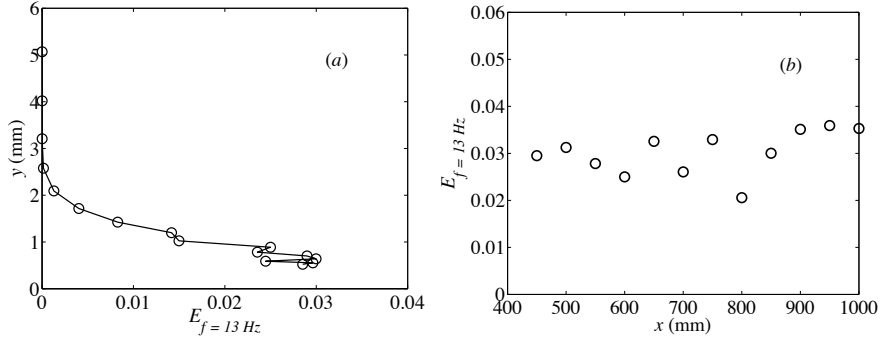


FIGURE A.2. Spatial dependence of the energy peak in (a) the wall-normal direction at $x = 550$ mm and (b) the streamwise direction at $y/\delta_1 \approx 1$.

that are unaffected by the vibration. The resulting boundary layer profiles for the different filtering frequencies are shown in figure A.3(b). Initially, there is a large drop in energy for a narrow bandwidth, which means that the energy in the vibrations is being filtered away. But eventually the filtering does not produce significant changes for a wider bandwidth, implying that the vibrational energy has been filtered away and now we are filtering out the energies unaffected by the vibration. The final bandwidth that was chosen was between 5 and 20 Hz. It can be seen that with a properly filtered signal a disturbance peak is clear at $y = 1$ mm whereas an unfiltered signal shows continuously increasing energy and thus the error in the disturbance amplitudes are greatly reduced.

f_{band}	Line style
unfiltered	—
10-15 Hz	—
5-20 Hz	- . -
5-25 Hz	- . -
1-20 Hz	- - -
1-25 Hz	- - -

TABLE 1. Filtering frequencies tested to reduce the effect of vibrations of the traversing mechanism.

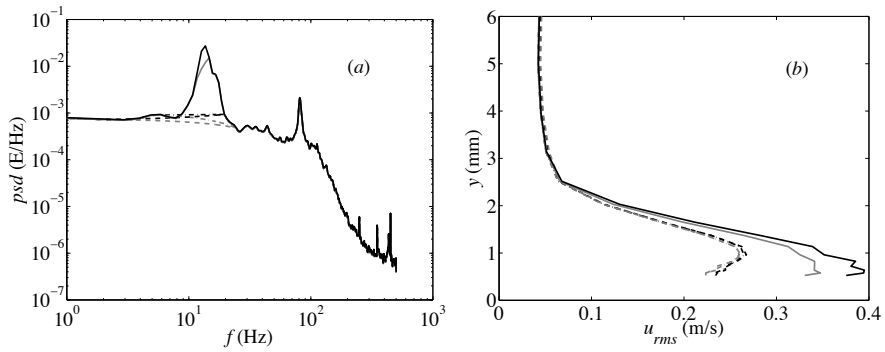


FIGURE A.3. (a) spectra of the original signal with those of different filtering frequencies. (b) The resulting boundary layer disturbance profile for different filtering frequencies. See table 1 for line style

It should be noted that filtering was needed only in the case of very low disturbance levels. For higher disturbance levels, such as those for larger initial turbulence intensities or in the boundary layers far downstream, the energy due to vibration was dwarfed by the energy due to the natural disturbances.

Acknowledgements

First of all I would like to thank my supervisors Prof. Henrik Alfredsson and Dr. Jens Fransson for accepting me as their student and their help and support in every part of this work.

Such large scale experiments cannot be done alone and I would like to thank all my colleagues in the lab who helped me with heavy lifting and heady discussions. Alessandro, Olle, Gabriele, Veronica, Bengt, Davide, Shahab, are only the start of a list that has grown too long over five years. Allan, Outi, Mathias and Karl are thanked for willing to venture out further than Valhallavägen for lunch. A special acknowledgment to my office mate of 5 years, Ramis Örlü, whose contributions to this work cannot be summarised well in such a small space. From teaching me how to build hot-wires to sharing the shear depth of your knowledge, I am truly indebted to you.

I would like to thank the technicians in the machine shop, Kim Karlström and Göran Rådberg as well as the earlier work of Marcus Gällstedt and Ulf Landen. With a rough description of what I needed they were able to produce results 100 times better than what I had originally imagined.

This work could not have been performed without the valuable input from my colleagues working on simulations and theory. David Templemann was responsible for the numerical calculations related to crossflow stability and I would like to thank him and Ardeshir Hanifi for very productive discussions as well as their ability to find excellent bars and restaurants in foreign cities. Additional discussions with Lars-Uve Schrader and Luca Brandt proved helpful and are gratefully acknowledged.

During my time here I was fortunate enough to participate in the collaborative effort, ICET. I am grateful to the hospitality of Prof. Hassan Nagib at IIT, Chicago and Prof. Ivan. Marusic and Prof. Min Chong at University of Melbourne along with their colleagues and students. I have also greatly enjoyed working closely with Prof. Masaharu Matsubara and Prof. Yoshiyuki Tsuji.

Financial support by the European Commission through the FP6 project "TELFONA" (Contract No AST4-CT-2005-516109) as well as the Linné Flow Centre is gratefully acknowledged.

If I don't make it, tell Helena, "Hello."

References

- ANDERSSON, P., BERGGREN, M. & HENNINGSON, D. S. 1999 Optimal disturbances and bypass transition in boundary layers. *Phys. Fluids* **11**, 134–150.
- ANDERSSON, P., BRANDT, L., BOTTARO, A. & HENNINGSON, D. S. 2001 On the breakdown of boundary layer streaks. *J. Fluid Mech.* **428**, 29–60.
- ASAI, M., MINAGAWA, M. & NISHIOKA, M. 2002 The instability and breakdown of a near-wall low-speed streak. *J. Fluid Mech.* **455**, 289–314.
- BERTOLOTTI, F. 2000 Receptivity of three-dimensional boundary-layers to localized wall roughness and suction. *Phys. Fluids* **12**, 1799–1808.
- BIPPES, H. 1999 Basic experiments on transition in three-dimensional boundary layers dominated by crossflow instability. *Prog. Aerosp. Sci.* **35**, 363–412.
- BIPPES, H. & LERCHE, T. 1997 Transition prediction in three-dimensional boundary-layer flows unstable to crossflow instability. *AIAA Paper* 1997–1906.
- BIPPES, H., MÜLLER, B. & WAGNER, M. 1991 Measurements and stability calculations of the disturbance growth in an unstable three-dimensional boundary layer. *Phys. Fluids A* **3**, 2371–2377.
- BUTLER, K. & FARRELL, B. F. 1992 Three-dimensional optimal perturbations in viscous shear flow. *Phys. Fluids A* **8**, 1637–1650.
- BYSTRÖM, M., LEVIN, O. & HENNINGSON, D. S. 2007 Optimal disturbances in suction boundary layers. *Eur. J. Mech./B Fluids* **26**, 330–343.
- CHERNORAY, V. C., A., DOVGAL, A. V., KOZLOV, V. V. & LÖFDAHL, L. 2005 Experiments on secondary instability of streamwise vortices in a swept-wing boundary layer. *J. Fluid Mech.* **534**, 295–325.
- COLLIS, S. & LELE, S. 1999 Receptivity to surface roughness near a swept leading edge. *J. Fluid Mech.* **380**, 141–168.
- CUTLER, A. & BRADSHAW, P. 1991 A crossed hot-wire technique for complex turbulent flows. *Exp. Fluids* **12**, 17–22.
- DEYHLE, H. 1993 Einfluss der äußeren Strömungsbedingungen auf den Transitionprozess einer dreidimensionalen Grenzschicht. *Ph.D Thesis* TH Hanover, published in: VDI Fortschritt-Bericht Reihe 7 No. 226, VDI-Verlag, Düsseldorf, Germany.

- DEYHLE, H., HÖHLER, G. & BIPPES, H. 1993 Experimental investigation of instability wave propagation in a three-dimensional boundary-layer flow. *AIAA J.* **31**, 637–645.
- FRANSSON, J. H. M. & CORBETT, P. 2003 Optimal linear growth in the asymptotic suction boundary layer. *Eur. J. Mech./B Fluids* **22**, 259–270.
- FRANSSON, J. H. M. & ALFREDSSON, P. H. 2003 On the disturbance growth in an asymptotic suction boundary layer. *J. Fluid Mech.* **482**, 51–90.
- FRANSSON, J. H. M., BRANDT, L., TALAMELLI, A. & COSSU, C. 2004 Experimental and theoretical investigation of the nonmodal growth of steady streaks in a flat plate boundary layer. *Phys. Fluids* **16**, 3627–3638.
- GOLDSTEIN, M. E. 1983 The evolution of Tollmien–Schlichting waves near a leading edge. *J. Fluid Mech.* **127**, 59–81.
- GOLDSTEIN, M. E. 1985 Scattering of acoustic waves into Tollmien–Schlichting waves by small streamwise variations in surface geometry. *J. Fluid Mech.* **154**, 509–529.
- HOCKING, L. 1975 Non-linear instability of the asymptotic suction velocity profile. *Quart. J. Mech. Appl. Math.* **28**, 341–353.
- HÖGBERG, M. & HENNINGSON, D. 1998 Secondary instability of cross-flow vortices in Falkner–Skan–Cooke boundary layers. *J. Fluid Mech.* **368**, 339–357.
- JOHANSSON, A. V. & ALFREDSSON, P. H. 1982 On the structure of turbulent channel flow. *J. Fluid Mech.* **122**, 295–314.
- KACHANOV, Y. 1994 Physical mechanisms of laminar–boundary-layer transition. *Annu. Rev. Fluid. Mech.* **26**, 411–482.
- KAWAKAMI, M., KOHAMA, Y. & OKUTSU, M. 1999 Stability characteristics of stationary crossflow vortices in three-dimensional boundary layer. *AIAA Paper* 1999–0811.
- KLEBANOFF, P., TIDSTROM, K. & SARGENT, L. M. 1962 The three-dimensional nature of boundary-layer instability. *J. Fluid Mech.* **12**, 1–34.
- KLEBANOFF, P. S. 1971 Effects of free-stream turbulence on a laminar boundary layer. *Bull. Am. Phys. Soc.* **16**.
- KURIAN, T. & FRANSSON, J. H. M. 2009 Grid-generated turbulence revisited. *Fluid Dyn. Res.* **41**, 021403. *PhD. Thesis, Paper 1.*
- KURIAN, T. & FRANSSON, J. H. M. 2010 Transient growth in the asymptotic suction boundary layer. *PhD. Thesis, Paper 3.*
- KURIAN, T., FRANSSON, J. H. M. & ALFREDSSON, P. H. 2010 Receptivity of cross-flow instabilities to free-stream turbulence and surface roughness. *PhD. Thesis, Paper 2.*
- LANDAHL, M. T. 1980 A note on an algebraic instability of inviscid parallel shear flows. *J. Fluid Mech.* **98**, 243–251.
- LINDGREN, B. & JOHANSSON, A. V. 2002 Evaluation of the flow quality in the MTL wind-tunnel. *Tech. Rep.* TRITA MEK 2002:13, KTH, Stockholm.
- LUCHINI, P. 1996 Reynolds-number-independent instability of the boundary layer over a flat surface. *J. Fluid Mech.* **327**, 101–115.
- LUCHINI, P. 2000 Reynolds-number-independent instability of the boundary layer over a flat surface: optimal perturbations. *J. Fluid Mech.* **404**, 289–309.
- MALIK, M., LI, F. & CHANG, C. 1994 Crossflow disturbances in three-dimensional

- boundary layers: nonlinear development, wave interaction and secondary instability. *J. Fluid Mech.* **268**, 1–36.
- MALIK, M., LI, F., CHOUDHARI, M. & CHANG, C. 1999 Secondary instability of crossflow vortices and swept-wing boundary-layer transition. *J. Fluid Mech.* **399**, 85–115.
- MATSUBARA, M. & ALFREDSSON, P. H. 2001 Disturbance growth in boundary layers subjected to free-stream turbulence. *J. Fluid Mech.* **430**, 149–168.
- MORKOVIN, M. V. 1969 Critical evaluation of transition from laminar to turbulent shear layer with emphasis on hypersonically traveling bodies. *Tech. Rep. AFFDL-TR-68-149*.
- MÜLLER, B. 1990 Experimental study of the travelling waves in a three-dimensional boundary layer. In *Laminar-Turbulent Transition, IUTAM Symp, Toulouse, France* (ed. D. Arnal & R. Michel) pp. 489–498. Springer-Verlag, Berlin
- NG, L. & CROUCH, J. 1999 Roughness-induced receptivity to crossflow vortices on a swept wing. *Phys. Fluids* **11**, 432–438.
- ÖSTERLUND, J. 1999 Experimental studies of zero pressure-gradient turbulent boundary layer flow. *PhD. Thesis TRITA MEK 1999:16*, KTH, Stockholm.
- RADEZTSKY, R., REIBERT, M. & SARIC, W. S. 1994 Development of stationary crossflow vortices on a swept wing. *AIAA Paper* 1994-2373.
- RADEZTSKY, R., REIBERT, M. & SARIC, W. S. 1999 Effect of isolated micron-sized roughness on transition in swept-wing flows. *AIAA J.* **37**, 1370–1377.
- REIBERT, M., SARIC, W. S., CARILLO JR, R. & CHAPMAN, K. 1996 Experiments in nonlinear saturation of stationary crossflow vortices in a swept-wing boundary layer. *AIAA Paper* 1996-0184.
- RESHOTKO, E. 2001 Transient growth: A factor in bypass transition. *Phys. Fluids* **13**, 1067–1075.
- REYNOLDS, O. 1883 An experimental investigation of the circumstances which determine whether the motion of water shall be direct or sinuous, and of the law of resistance in parallel channel. *R. Soc. Lond. Phil. Trans. A.* **174**, 935–982.
- SARIC, W. S., REED, H. L. & KERSCHEN, E. 2002 Boundary-layer receptivity to freestream disturbances. *Annu. Rev. Fluid. Mech.* **34**, 291–319.
- SARIC, W. S., REED, H. L. & WHITE, E. B. 2003 Stability and transition of three-dimensional boundary layers. *Annu. Rev. Fluid. Mech.* **35**, 413–440.
- SARIC, W. S. & YEATES, L. 1985 Experiments on the stability of crossflow vortices in swept-wing flows. *AIAA Paper* 1985-0493.
- SCHLICHTING, H. 1979 *Boundary Layer Theory*. 7th ed. McGraw-Hill, New York.
- SCHMID, P. J. & HENNINGSON, D. S. 2001 *Stability and transition in shear flows*. Springer-Verlag, New York.
- SCHRADER, L.-U., BRANDT, L. & HENNINGSON, D. S. 2009 Receptivity mechanisms in three-dimensional boundary-layer flows. *J. Fluid Mech.* **618**, 209–241.
- SCHUBAUER, G. & SKRAMSTAD, H. 1948 Laminar-boundary-layer oscillations and transition on a flat plate. *NACA Tech. Rep.* No. 909.
- TEMPELMANN, D., HANIFI, A. & HENNINGSON, D. S. 2010 Spatial optimal growth in three-dimensional boundary layers. *J. Fluid. Mech.* **646**, 5–37.

- VOGEL, S. 1996 *Life in moving fluids: the physical biology of flow*. 2nd ed. Princeton University Press, Princeton.
- WANDERLEY, J. & CORKE, T. 2001 Boundary layer receptivity to free-stream sound on elliptic leading edges of flat plates. *J. Fluid Mech.* **429**, 1–21.
- WEGENER, P. P. 1997 *What makes airplanes fly?: history, science, and applications of aerodynamics*. 2nd ed. Springer–Verlag, New York.
- WESTIN, K., BAKCHINOV, A., KOZLOV, V. & ALFREDSSON, P. H. 1998 Experiments on localized disturbances in a flat plate boundary layer. Part 1. The receptivity and evolution of a localized free stream disturbance. *Eur. J. Mech./B Fluids* **17**, 823–846.
- WESTIN, K., BOIKO, A., KLINGMANN, B., KOZLOV, V. & ALFREDSSON, P. H. 1994 Experiments in a boundary layer subjected to free stream turbulence. part 1. boundary layer structure and receptivity. *J. Fluid Mech.* **281**, 193–218.
- WHITE, E. & ERGIN, F. 2003 Receptivity and transient growth of roughness-induced disturbances. *AIAA Paper* 2003–4243.
- WHITE, E. & SARIC, W. S. 2005 Secondary instability of crossflow vortices. *J. Fluid Mech.* **525**, 275–308.
- WHITE, E. B. 2002 Transient growth of stationary disturbances in a flat plate boundary layer. *Phys. Fluids* **14**, 4429–4439.
- WHITE, E. B., RICE, J. & ERGIN, F. G. 2005 Receptivity of stationary transient disturbances to surface roughness. *Phys. Fluids* **17**, 064109.
- YOSHIOKA, S., FRANSSON, J. H. M. & ALFREDSSON, P. H. 2004 Free stream turbulence induced disturbances in boundary layers with wall suction. *Phys. Fluids* **16**, 3530–3539.

